ELSEVIER

Journal of Nuclear Materials 290–293 (2001) 1023–1029

journal of nuclear materials

www.elsevier.nl/locate/jnucmat

Section 9. Long pulse experiments

Active cooling, calorimetry and energy balance in Tore Supra

J.C. Vallet *, R. Reichle, M. Chantant, V. Basiuk, R. Mitteau

DRFC, Association Euratom-CEA sur la Fusion contrôlée, CE Cadarache, F13108 Saint-Paul-Lez-Durance, France

Abstract

The active cooling of the Tore Supra plasma facing components, including its operational limits, is extensively described. The associated calorimetric diagnostic is found to be a powerful and accurate tool to study the energy balance of plasma discharges.

Keywords: Calorimetry; Energy balance; Power balance

1. Introduction

Tore Supra will remain the only tokamak built at the very end of the 20th century to face the major technological challenges underlying the design of a thermonuclear reactor. For Tore Supra, these challenges focus on the control of full steady-state quasi-thermonuclear plasmas, on a time scale of the order of few hundred seconds. Among the very specific systems required to reach this goal, some on Tore Supra, have already been brightly highlighted, the famous being the cryomagnetic system. It requires specific thermal screens and insulation materials, making possible the neighboring of the most extreme temperatures: few 10^7 K on plasma axis and 1.7 K in the helium bath inside the toroïdal field coils. Another is the plasma heat removal system based on actively cooled plasma-facing components (pfcs).

The active cooling of all the pfcs is provided by the pressurized water loop (PWL30). The various screens and pfcs correspond to about 50 elements connected in parallel to the PWL30, providing, in principle, the capability to extract all the input energy. Each element is diagnosed. This makes of Tore Supra a unique tool to study the energy balance of plasma discharges as well as the spatial distribution of the output plasma fluxes.

This paper is divided into three parts. In the first one, the PWL30, including its operational regime, instrumentation and calorimetric measurements, is extensively described. The second part is devoted to the calorimetric analysis. The influence of the ripple losses and of the RF power calibration will be analyzed. In the third part, the difficulty encountered to produce long plasma pulses will be recalled. The main operating problems of an actively cooled tokamak, i.e. the in-vessel water leaks – will be briefly analyzed.

2. Cooling system and calorimetric measurements

The PWL30 is made of two parts. The in-vessel part is a hydraulic net where the pfcs are connected in parallel. The external part is essentially made of a single pipe, onto which the different systems needed to operate the loop are installed: the pressurizer, the heat exchanger, the electrical heater and the pump (Fig. 1). The mass of the circulating water is about 18.5 tons, pressurized to about 28 bars. During plasma operation the mass flow is about 280 ton/h. The electrical heater is used to bake out the vessel up to 200°C. The heat exchanger, so far, due to its limiting working flow (30 ton/h) is only used after baking to cool down the water of the loop to 150°C before the beginning of each experimental session. During plasma operation, the behavior of the coolant temperature is the result of the competition between the thermal losses of the PWL30 – typically 45 kW or 2°C/h at 150°C – and the energy gained during plasma discharges.

The actively cooled components can be classified in five groups: (1) The thermal screens (SCR) include the

* Corresponding author. Tel.: +33-442 256 162; fax: +33-442 256 233.

E-mail address: vallet@drfc.cad.cea.fr (J.C. Vallet).

0022-3115/01/$ - see front matter
PII: S0022-3115(00)00494-3

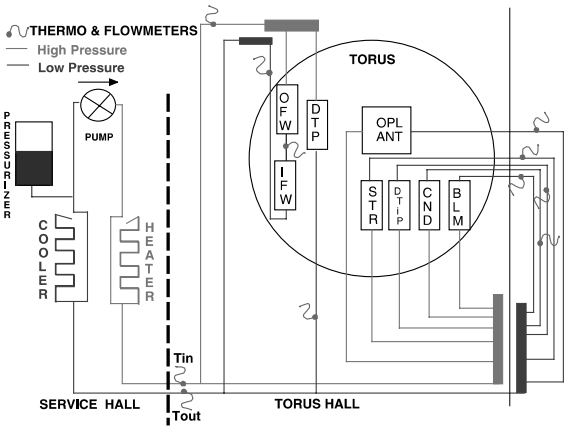

Fig. 1. Sketch of the PWL30. The arrow on the pump gives the flow direction.

inner first wall (IFW) and the outer first wall (OFW), respectively, located on the high and low field side. They cover the most part of the vacuum vessel, except for small gaps in between and the apertures of the ports, appearing as holes in the OFW. The IFW can be used as a toroïdal limiter. The OFW, always at least 10 cm away from the plasma boundary, receives only radiated and charge exchange fluxes. (2) The ergodic divertor (ED) is made of six magnetic coils installed in front of the OFW. Each coil integrates mechanical structures (STRs), target plates (DTPs), conducting wires (CNDs) and Titanium pumps (DTiPs). (3) The limiters (LIMs) with two subgroups: the outboard pump limiter (OPL) installed in a mid-plane port and the bottom limiters (BLMs). (4) The RF antennae (ANT) groups with two lower hybrid (LH) grills and three ion cyclotron range frequency (ICRF) antennae. (5) The calorimetric ripple loss collectors (RIPs), installed in two vertical ports, one, in a bottom port, collecting fast electrons and one in a top port collecting fast ions. Table 1 indicates the number of independent hydraulic elements N, the flow Γ and the cooling time constant τ_C for each component.

The PWL30 is equipped with temperature probes and flowmeters, in such a way that both global and element by element calorimetric analysis can be made. Temperature probe locations are schematically given in Fig. 1. The global calorimetric measurements are made from two temperature probes, called T_{in} and T_{out}, immersed in the external pipe, respectively, upstream and downstream of the parallel net. Each element, 'i', is equipped with a temperature probe measuring, T_i, the output temperature of the coolant before mixing. Temperature probes are K type thermocouples, with a sensitivity 40 μV/°C, and absolute accuracy ±1.5°C, directly immersed in the coolant, typical rise time 0.8 s. Flowmeters are based on differential pressure measurement, accuracy ±2%. The measurement of the flow in each element is possible. Fifteen flow transmitters are simultaneously available. Before each experimental campaign, a flow table giving the ratio of the flow in each element to the total flow is established. Moreover, the validity of this table can be verified on each shot analyzing the heat pulse propagation throughout the hydraulic circuit. Typical values for the transit time τ_1 and τ_2, respectively, from T_{in} to T_i and from T_i to T_{out} are given in Table 1 for a total flow of 280 ton/h. About 65 calorimetric measurements are recorded for each shot during an

Table 1
Some characteristics of the actively cooled components

CAT.	Comp.	N	Flow (ton/h)	$\tau_c(s)$	$\tau_1(s)$	$\tau_2(s)$
SCR	OFW	6	61.1	9	65	40
	IFW	6		45	45	60
ED	DTP	6	63.2	5	22	28
	STR	6	12.2	128	20	100
	CND	6	5.2	30	30	160
	DTiP	6	6.6	11	25	80
LIM	OPL	1	5.4	313	50	120
	BLM	4	17.1	–	40	60
ANT	LH1	1	4.1	8	40	60
	LH2	1	27.8	8	35	60
	ICRF1	1	23.6	8	35	59
	ICRF2	1	11.4	7	35	52
	ICRF3	1	23.6	6	35	59
RIP	ION	1	15.3	–	–	–
	ELEC	1	2.4	–	–	–
Sum	PWL30	48	277	–	–	–

acquisition window of 480 s, i.e. two cycles time of the coolant in the PWL30 – starting about 30 s before the breakdown of the plasma. So far, the heat exchanger not being used, it is observed that the extracted heat measured at a time t on T_{out} is detected τ_{out} later on T_{in}. $\tau_{out} \sim 120$ s is the transit time of the coolant in the external pipe. This phenomenon is called the 'hot water pulse'. Though it makes the calorimetric analysis more complicated, it has been found to be very useful to measure the various transit times and also to verify the low level of the in-vessel thermal losses. The flows being constant in time, a typical behavior of the time variation of the thermal power P circulating in the PWL30 (Fig. 2(a)), measured on T_{in} and T_{out}, and on each component (Fig. 2(b)) is shown in Fig. 2 with $P_i = C_p \Gamma_i (T_i(t) - T_i(0))$. T_i stands either for T_{in}, T_{out} or for the averaged temperature of a given component. Γ_i is the corresponding flow. For comparison with P_{out}, the P_i displayed on Fig. 2 (b) have been translated with respect to their transit time, τ_{2i}, (see Table 1). The Fig. 2(a) also shows, for comparison with P_{out}, the behavior of $\text{Scomp} = \sum_i P_i(t + \tau_{2i})$. To get an optimal comparison, the heat diffusion into the coolant has been taken into account. To avoid writing the energy balance as a sum of 50 terms, the global analysis from T_{in} and T_{out} has been preferred. Doing this, due to the thermal dilution, one is facing the problem of the temperature measurement sensitivity. Previously, the temperatures have been measured with industrial equipment limiting the sensitivity to a digital noise level corresponding to ± 0.2°C. Such sensitivity has restricted accurate calorimetric analysis to discharges with input energy larger than 50 MJ. A statistical analysis performed on ohmic shots has shown that the sensitivity of the temperature measurements could be largely improved. Then a better electronics has been developed, providing a sensitivity limit of the order of ± 0.02°C

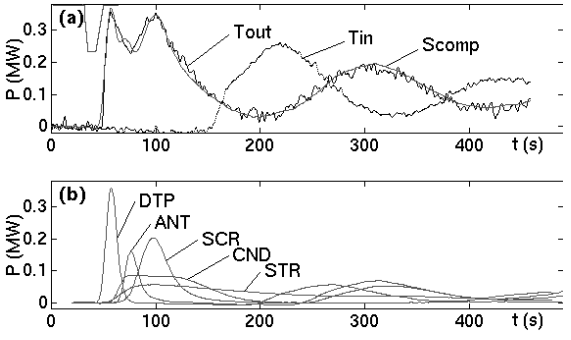

Fig. 2. Global and pfcs calorimetric measurements. TS28228 ED shot with ICRH: (a) Global extracted power T_{out}. T_{in} shows the hot water pulse beyond $t \sim 150$ s. (b) Thermal power P_i extracted from each component.

3. Calorimetric analysis and energy balance

The energy balance is the result of the comparison of the total input energy, E_{in}, measured from the power sources – with the total dissipated energy, E_{out}, partly measured and partly estimated from the calorimetric data. The larger part of E_{out} is the energy extracted by the PWL30: E_{L30}. With the improved temperature measurements, reliable estimate of E_{L30} can be done down to 10 MJ. Thermocouples having an absolute accuracy of ± 1.5°C and recording temperature variations of the order of 0.5°C for ohmic shot, only the temperature variations can be considered. This fact raises the problem of the estimate of the in-vessel thermal losses. It is possible to eliminate the 'static' thermal losses by merging the offsets of the two measurements. However, during plasma experiments, some in-vessel 'transient' losses could appear, due to the thermal excursion of the coolant. These losses have been checked, analyzing the hot water pulse. If one considers high energy input discharges, typically $E_{L30} \sim 100$ MJ, (Fig. 3) for which the signal to noise ratio is such that the determination of the offset, $\overline{\text{off}}$, is straightforward, one observes that, on $E_{L30}(t) = \int_0^t \mathrm{d}u \Gamma C_p (T_{out}(u) - T_{in}(u + \bar{\tau}) - \overline{\text{off}})$, an oscillation appears during the hot water pulse. Now, if one takes into account the spreading of the hot water pulse due to the differential transit time throughout the components by substituting

$$T_{is}(t + \bar{\tau}) = \sum_i T_{in}(t + \tau_i) \frac{\Gamma_1}{\Gamma_{L30}} + \text{off}$$

to $T_{in} + \text{off}$, where τ_i and Γ_i are, respectively, the total in-vessel transit time and the flow for each component 'i', a completely flat behavior of E_{L30} is obtained during the hot water pulse.This point indicates that the transient losses are negligible. The time behavior of the E_{L30} is almost 'universal', and it depends more on the characteristics of the components than on the total input energy. In fact, for the very low input energy discharges,

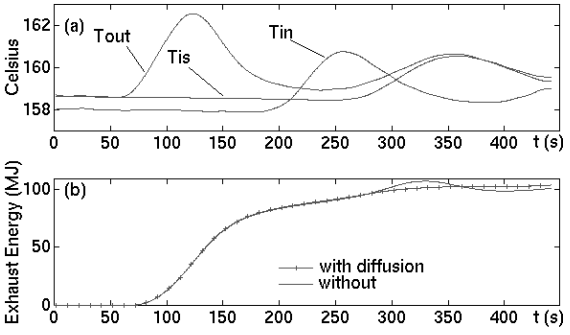

Fig. 3. E_{L30} estimate. High-energy shot $E_{L30} \sim 100$ MJ: (a) T_{in}, T_{out} and $T_i s$; (b) E_{L30} estimate with and without the hot water pulse diffusion.

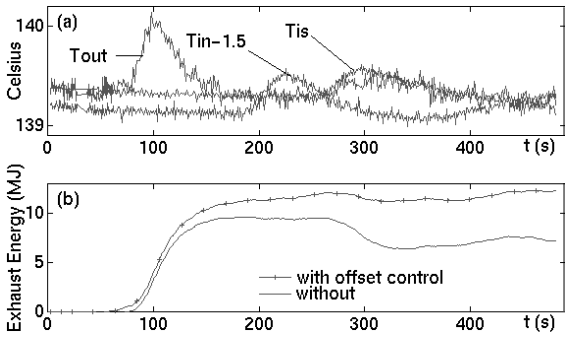

Fig. 4. E_{L30} estimate. Low-energy ohmic shot $E_{L30} \sim 12$ MJ. The offset off is adjusted to reproduce a behavior of E_{L30} as close as possible to the high-energy case.

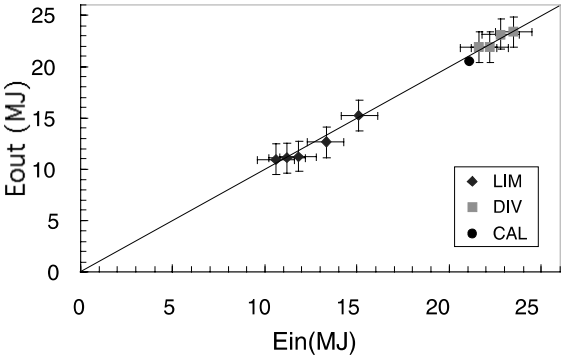

Fig. 5. Ohmic energy balance for limiter and ED shots. The calibration point (CAL) is obtained feeding the ED coils without plasma.

$E_{L30} < 20$ MJ, the estimate of, $\overline{\text{off}}$, has to be done with an accuracy of the order of 0.01°C. Thus in this case, the estimate of $\overline{\text{off}}$ is chosen to provide a behavior of E_{L30} closest to the one found for high-energy discharges (Fig. 4).

For ohmic discharges, the total input energy is $E_{in} = E_{OH} + E_{ED}$, where E_{OH} is the ohmic energy calculated from magnetic measurements and E_{ED} is the electrical energy dissipated in the ED coils. E_{out} is the sum of four terms, $E_{out} = E_{L30} + E^{rad}_{vess} + E^{\infty}_{STR} + E^{\infty}_{OPL}$. $E^{rad}_{vess} \sim 0.7E_{OFW}$ is the radiated energy reaching the vacuum vessel wall due to the incomplete coverage of the OFW. E_{OFW} is the energy removed from the OFW. The factor 0.7 is the ratio of ports and gaps area to the exposed area of the OFW. The two last terms E^{∞}_{STR} and E^{∞}_{OPL} correspond to the part of the thermal energy, stored in the semi-inertial components STR and OPL, which is released on a time scale longer than the acquisition window. These terms are calculated by e-folding extrapolation, time integrations being done from 250 s to infinite. One finds that $E^{\infty}_{STR} \approx 0.4E_{STR}$ and $E^{\infty}_{OPL} \approx 1.3E_{OPL}$, where E_{STR} and E_{OPL} are the energies extracted from the semi-inertial components up to $t = 250$ s. In ohmic regime the energy balance can be written:

$$E_{OH} + E_{ED} = E_{L30} + 0.7E_{OFW} + 0.4E_{STR} + 1.3E_{OPL}.$$

Following this procedure, for ohmic shots, one gets a good coherence between the measurements of the input and output energies (Fig. 5 and Table 2).

If, for ohmic plasmas, the input and output energies are well balanced, the result is quite different for RF heating experiments. On Tore Supra the auxiliary power sources are RF only. In the range of 42–56 MHz – ICRF, 6 MW generator – the more commonly used heating scenario is ICRH Hmin. At 3.7 GHz – LH, 8 MW generator – the RF power is used for current drive experiments – LHCD. RF power and heating scenarios introduce two questions. First, the estimate of the RF power injected inside the torus, based on RF measurements, is known to be difficult and may present quite a large error. Second, new types of losses appear, and have to be quantified. Such losses may be the direct RF losses, i.e. RF power escaping from the torus – or in the experimental scenarios considered here – generating fast particles, the ripple losses. The latter may either intercept the thermal screens or enter into the 12 vertical ports. During the last experimental campaign, to study the ripple losses two sets of diagnostics, electrostatic and calorimetric collectors [1], were, respectively, available for ions and electrons. They provide, respectively, the

Table 2
Calorimetric results of ohmic energy balance analysis, $F_{cal} = E_{out}/E_{in}$

Shot	Type	E_{OH}	E_{ED}	E_{in}	off	E_{L30}	E_{OFW}	E_{STR}	E_{OPL}	E_{out}	F_{cal}
27759	OH/IFW	11.2	0	11.20	−0.03	10.4	0.6	0.4	0.1	11.1	0.99
27760	OH/IFW	10.6	0	10.60	−0.02	10.3	0.6	0.4	0.1	11.0	1.03
27764	OH/IFW	13.3	0	13.30	−0.03	11.6	0.7	0.4	0.3	12.7	0.95
27786	OH/IFW	15.1	0	15.10	−0.02	13.2	1.6	1.3	0.2	15.2	1.01
OHLM99	CUMIFW	11.8	0	11.80	−0.02	10.5	0.7	0.4	0.1	11.3	0.95
27839	OH/DIV	15.4	6.8	22.20	0.02	19.0	1.2	2.3	0.8	21.9	0.99
27909	OH/DIV	14.9	6.7	21.60	0.05	19.1	1.2	3.2	0.3	21.9	1.01
28030	OH/DIV	16.7	6.1	22.80	−0.01	20	1.5	3.7	0.2	23.1	1.01
28031	OH/DIV	17.2	6.3	23.50	0.05	20	1.9	3.6	0.2	23.4	0.99

number of trapped particles $N_{\rm rip}$ and the thermal energy $E_{\rm rip}$, entering into a port. The total particle number and the total lost energy are assumed to be 18 times the measured values – 18 being the number of toroïdal field coils. The calorimetric deficits due to the ripple are assumed to be 11 times the measured energies $E_{\rm rip}$. This assumption of the symmetry of the ripple losses can be partly verified, when power is delivered from different antennae installed at different toroïdal locations with respect to the location of the collectors [2]. During the last campaign, it has been found that the average energy per lost ion $\overline{E}_i = E^i_{\rm rip}/N_{\rm rip}$ is 2.5–3.5 larger than a previous estimate [1], and corresponds to global ion ripple losses $E^i_{\rm rip}$ varying between 10% and 30% of the ICRH power [2]. Electron ripple losses $E^e_{\rm rip}$ are always lower than 10%.

The energy balance with RF heating power can finally be written: $E_{\rm in} = E_{\rm out}$

$$\begin{aligned} \text{with}\quad & E_{\rm in} = E_{\rm OH} + E_{\rm ED} + (E_{\rm ICRH} - E^{\rm miss}_{\rm ICRH}) \\ & \quad + (E_{\rm LH} - E^{\rm miss}_{\rm LH}), \\ \text{and}\quad & E_{\rm out} = E_{\rm L30} + 0.7E_{\rm OFW} + 0.4E_{\rm STR} \\ & \quad + 1.3E_{\rm OPL} + 11E^i_{\rm rip} + 11E^e_{\rm rip}, \end{aligned}$$

where $E_{\rm ICRH}$ and $E_{\rm LH}$ are the ICRH and the LH input power obtained from RF measurements. $E^{\rm miss}_{\rm ICRH}$ and $E^{\rm miss}_{\rm LH}$ are the expected missing energies including direct RF loss terms and eventual inaccuracy of RF power estimate. These two terms, so far, cannot be directly estimated except from the energy balance itself, applied to separated heating experiments (Figs. 6(a) and (b)). For ICRH, (Fig. 6(a)) the part of the auxiliary energies which are effectively coupled to the plasma: $(E_{\rm ICRH} - E^{\rm miss}_{\rm ICRH}) = E_{\rm out} - E_{\rm OH} - E_{\rm ED}$ is plotted versus $E_{\rm ICRH}$. The assumption is that, as shown for ohmic shots, the component $E_{\rm OH} + E_{\rm ED}$ of the total input energy is fully recovered. Then, one finds that $E^{\rm miss}_{\rm ICRH}$ is of the order of 20% of $E_{\rm ICRH}$ (Fig. 6(a)). This value seems too high to be only due to direct RF losses and points out the problem of the ICRH power calibration. Fig. 6(a), the total energy lost by ripple ions, $18 * E^i_{\rm rip}$, is also plotted versus $E_{\rm ICRH}$. The same study made for LH shows the same characteristics (Fig. 6(b)).

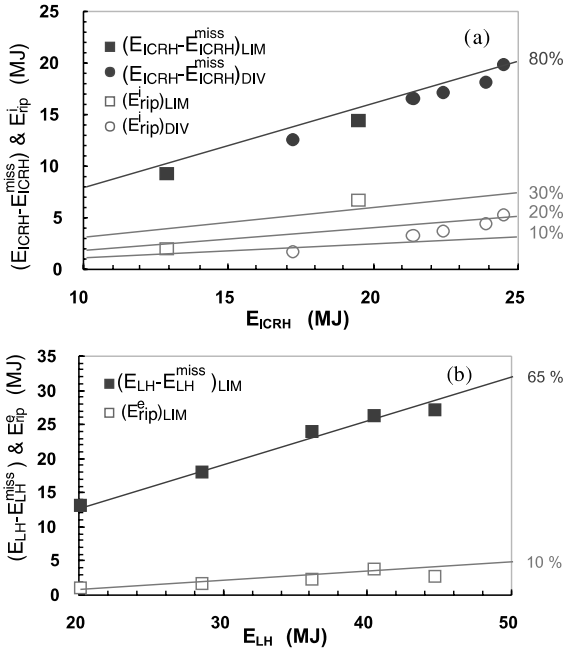

Fig. 6. Energy balance with additional heating: (a) ICRH, (b) LHCD. The missing part of the additinal energy and the total ripple loss energy are plotted versus the heating power.

The global energy balance presented above, for ICRH ED shots, confirms the existence of an overestimate of the total input energy previously deduced from the power balance analysis. The power balance can be written

$$P_{\rm bal} = (P_{\rm OH} + P_{\rm ICRH} - {\rm d}W/{\rm d}t) - (P_{\rm rad} + P_{\rm cond}),$$

where $P_{\rm OH}$ and $P_{\rm ICRH}$ are, respectively, the ohmic and ICRH power, ${\rm d}W/{\rm d}t$ is the time derivative of the plasma stored energy. $P_{\rm rad}$ and $P_{\rm cond}$ are the estimates of the total radiated and conducted powers, respectively, obtained from the analysis of the bolometry and IR thermography. Statistical analyses have shown that though Pbal is close to zero in ohmic regime, it remains largely positive during ICRH. Pbal is found to be of the order of 30–40% of the ICRH power [3,4]. A good agreement is thus found with the calorimetric energy balance.

In addition to the global energy balance analysis, the calorimetry of the actively cooled components, made of diagnosed elements having finite poloïdal and toroïdal extent, can be used to study the local heat depositions. These studies gave results in four fields. Firstly, they contributed to solve the problem of the artifact appearing on top port bolometer arrays, during ICRH Hmin experiments. It has been found that this artifact is due to charge exchange reactions occurring between ripple ions and the residual neutral gas present in the port [5]. Secondly, it has been possible to address the problem of the $3D$ structure of the plasma emissivity in ED experiments [4,6,7]. In particular it is found that the total radiated power $P_{\rm rad} \sim f_{\rm p}$. $P_{\rm radh}$ is larger than the estimate provides by the horizontal bolometer array $P_{\rm radh}$, by a factor $f_{\rm p}$ defined as the toroïdal peaking factor. Typically, one finds that $f_{\rm p}$ is varying between 1 and 1.8 depending on plasma parameters such as the density and the plasma impurity content [4]. Thirdly, it is possible to study the splitting of the conductive flux between the ED target plates and the ED coil structures, respectively, 30% and 70%, and also to determine an e-folding decay length of the heat flux $\lambda_q \sim 25$ mm in

ohmic ED experiments. Results are qualitatively in agreement with those found in [8]. Fourthly, for plasma leaning on the IFW the calorimetric analysis of the six IFW panels allows to deduce an estimate of $\lambda_q \sim 12$ mm. This result has to be included in a more complete analysis, requiring an abnormal component to explain the poloïdal structure of the heat deposition on the IFW [9,10]

4. Limits of the Tore Supra cooling system

On Tore Supra the increase of the plasma pulse length is based on the capability of the LH power to drive the plasma current. It is known that the LH current drive, at constant LH power, decreases with density. Ultimately, at high input energy, it appears that the pulse length is bounded by an uncontrolled density rise. The detailed analysis shows that this is due to desorbed water trapped in the walls of the ports. These uncooled and poorly conditioned surfaces can be heated by energy fluxes arising from the plasma [11]. Reconsidering the problem of the ripple losses, one finds that the energy introduced in the vertical ports by fast particles is at least 10 times higher than from plasma radiation. This phenomenon is probably more efficient to desorb trapped water than the plasma radiation previously proposed as the main reason [11]. However, whatever the mechanism, the conclusion remains unchanged. To extend the plasma pulse length, each part of the machine receiving energy fluxes has to be efficiently conditioned and must have a controlled thermal excursion.

In a tokamak where all the pfcs are actively cooled, the major problem is the in-vessel water leak. Principally, such leaks can have three different origins: disruptions, control of safety variables or flux excursion on pfcs exceeding the design values. During about 12 years of experiments, Tore Supra had to face more than 15 water leaks due to plasma operation [12]. Concerning disruptions, two types of problems have been encountered: Firstly, electromechanical forces on water pipes are not to be underestimated. Secondly, it was found that the runaway production has to be minimized and managed, ultimately, bumpers such as the OPL, are designed to intercept and withstand the runaway flux. Concerning the management of the safety variables, one can note that the PWL30 safety is fully passive. The pfcs, expected to be thermally loaded or not, are fed according to their nominal request. This, though it often complicates the calorimetric analysis, is found to be very reliable for the pfcs safety. This has been clearly illustrated during the test of an actively cooled limiter having a cooling request incompatible with the PWL30 parameters: $T \sim 50$°C during shots. Thus, this limiter has been fed by an independent and configurable cooling loop. The test abruptly ended, when a fault in the safety parameter management led to use it without coolant flow in it, then destroying the component. The last water leak, which prematurely ended the last experimental campaign, has recalled that it can be hazardous to explore some unknown parameter domain – in this case, the low plasma density with high LHCD power – without a reliable surface temperature measurement of the more thermally loaded components. In this example, a very thin electron beam has led to an abnormal flux deposition on the most exposed tile of the IFW (ahead of only 0.2 mm from the surrounding), leading probably to an excess flux event. In the context of the imminent CIEL project [13], this has re-emphasized that an IR thermographic system is absolutely needed to ensure the safety of very advanced pfcs.

5. Conclusions

Tore Supra, with the present in-vessel components, has reached its operational limits, in terms of long pulse and heat removal capability. At moderate input power $P_{\text{in}} < 6$ MW, the limiting factor is rather the incomplete coverage of the vacuum vessel than the active cooling system.

Provided that the temperature measurements are sensitive enough, the calorimetric diagnostic coupled to the cooling system is found to be a very fruitful and accurate tool to study the energy balance. It allowed accurate quantifying of the ions and electron ripple loss rates. It allowed pointing out the problem of the estimate of the RF power injected inside the torus. On Tore Supra the RF sources, which are able to deliver very long pulses, are also actively cooled by a dedicated pressurized water loop. An upgrade of the coupled calorimetric diagnostic will allow in the very near future to get an absolute calorimetric calibration of the RF measurements. In addition to the global energy balance, the calorimetric diagnostic allows a spatially resolved analysis of the energy deposition on the discrete elements of the pfcs, and this both for conductive and radiative fluxes.

The daily management of an actively cooled tokamak, and the need to face the difficult problem of the in-vessel water leaks have allowed developing a genuine culture of the thermohydraulic safety of the actively cooled pfcs. This unique experience leads now to the completion of the CIEL project. The masterpiece of which, the Toroïdal Pumped Limiter is a high heat flux component, designed to extract 15 MW steady-state conductive power, with steady-state localized heat flux up to 10 MW/m^2. In this context the cooling system will continue to play a major role in Tore Supra. It is planned that, by the end of 2002, the mass flow of the PWL30 will reach 1100 ton/h, allowing the nominal performances of the CIEL components with an enlarged safety margin.

References

[1] V. Basiuk et al., Nucl. Fus. 35 (12) (1995) 1593.
[2] V. Basiuk et al., in: Proceedings of the 27th EPS Conference on Control Fusion and Plasma Physics, to appear.
[3] R. Reichle et al., in: Proceedings of the 25th EPS Conference on Control Fusion and Plasma Physics, Praha, ECA, vol. 22C, 1998, p. 631.
[4] R. Reichle et al., in Proceedings of the 26th EPS Conference on Control Fusion and Plasma Physics, Maastricht, Netherlands, ECA, vol. 23J, 1999, p. 973.
[5] J.-C. Vallet et al., in: Proceedings of the 26 EPS Conference on Control Fusion and Plasma Physics, Maastricht, Netherlands, ECA, vol. 23J, 1999, p. 1037.
[6] F. Laugier et al., contribution P2.54, these Proceedings.
[7] Y. Corre et al., contribution P2.55, these Proceedings.
[8] B. Meslin et al., in: Proceedings of the 24th Conference on Control Fusion and Plasma Physics, Berchtesgaden, ECA, vol. 21A-I, 1997, p. 197.
[9] R. Mitteau et al., in: Proceedings of the 26th EPS Conference on Control Fusion and Plasma Physics, Maastricht, Netherlands, ECA, vol. 23J, 1999, p. 673.
[10] R. Mitteau et al., Contribution P1.68, these Proceedings.
[11] C. Grisolia, J. Nucl. Mater. 266–269 (1999) 146.
[12] J.-J. Cordier et al., in: Proceedings of the 5th International Symposium on Fusion Nuclear Technology, Roma, September 1999.
[13] P. Garin, in: B. Beaumont, P. Libeyre, B. de Gentile, G. Tonon (Eds.), Proceedings of the 20th SOFT, Fusion Technology 1998, vol. 2, St. Paul Lez Durance, 1998, p. 1709.